Mobility, Miscibility, and Microdomain Structure in Nanostructured Thermoset Blends of Epoxy Resin and Amphiphilic Poly(ethylene oxide)-*block*-poly(propylene oxide)-*block*-poly(ethylene oxide) Triblock Copolymers Characterized by Solid-State NMR

Pingchuan Sun,[†] Qinqin Dang,[†] Baohui Li,[‡] Tiehong Chen,*[,†] Yinong Wang,[†] Hai Lin,[†] Qinghua Jin,[‡] and Datong Ding[‡]

Key Laboratory of Functional Polymer Materials for Adsorption and Separation, College of Chemistry and College of Physics, Nankai University, Tianjin, 300071, China

An-Chang Shi

Department of Physics and Astronomy, McMaster University, Hamilton, Ontario L8S 4M1, Canada

Received March 21, 2005; Revised Manuscript Received April 29, 2005

ABSTRACT: Solid-state NMR methods were used to characterize the heterogeneous dynamics, miscibility, and microdomain structure in nanostructured thermoset blends of epoxy resin (ER) and amphiphilic poly(ethylene oxide)-*block*-poly(propylene oxide)-*block*-poly(ethylene oxide) triblock copolymers (PEO−PPO−PEO). NMR experiments show that there is a distinct dynamic difference between the block copolymer (both PEO and PPO) and cured-ER matrix indicating the presence of phase separation, which also confirms the existence of the interphase region including a considerable amount of immobilized PEO and mobilized partially cured ER. An improved method based on spin-diffusion experiments enabled a quantitative determination of the interphase thickness. It is shown that a large percentage of PEO were intimately mixed with ER in the interphase region of the blends, while the rest mobile PEO and all PPO segregated from the ER network. It is observed that the domain size and long period depend strongly on the PEO fraction in the copolymers, whereas the interphase thickness of the blends is not sensitive to the PEO fraction. These NMR results unambiguously demonstrated that PEO blocks were only partially miscible with cured-ER network. Upon curing, the cross-linked rigid ER formed a separated microphase, while some PEO were locally expelled out of the cured-ER network and forms another microphase with PPO. The residual immobilized PEO were intimately mixed with some partially cured-ER matrix and formed the interphase region.

Introduction

The preparation and characterization of nanostructured polymeric materials have attracted significant attention in the past decade.[1] For example, it is well established that block copolymers self-assemble to form a variety of morphologies such as spherical, cylindrical, lamellar, and gyroid phase.[2] Furthermore, blending block copolymers with thermoplastic homopolymers have been widely employed to produce polymeric materials with different nanoscale structures.[3] However, few works had been reported on preparing nanostructured blends of thermoset homopolymers with block copolymers prior to the motivating work of Bates and co-workers in 1997.[4] Recently, toughening of the thermosetting resin by means of block copolymers has attracted significant attention.[5−7] It has been reported that the nanostructured thermoset blends exhibit unique nanostructure, morphologies, phase behavior, and physical properties.[4,5] In the block copolymer/thermoset blend, the final structure and morphologies of the blend are determined by several factors including the cross-linking reaction of the thermosetting resin, the self-assembly of the block copolymer, and the phase separation of the blend.[5,6] Naturally, such intrinsic competing interactions would have an impact on the final structures and properties of the blend.

Miscibility in polymer blends has received substantial attention in the past decade.[8] Although blends of epoxy resin and PEO-containing amphiphilic block copolymers have been studied by several groups,[4−7,9] the miscibility of PEO block with cured-ER network as well as the component dynamics and the interphase structure in these thermoset blends has not been well understood so far. There are two competing viewpoints concerning the miscibility of PEO block with the cured-ER network. In a study of ER/PEO−PPO−PEO blends using DSC measurements, Guo et al.[7] concluded that the PEO blocks were completely dissolved in the cured-ER network; thus, the PEO was considered to be completely miscible with the cured-ER. On the other hand, in the work on diblock copolymer PEO−PPO/ER blends, Mijovic et al.[6] concluded that the PEO gradually separated from the cured-ER network during some "critical" stage of cure. In another work on poly(ethylene oxide)-*block*-poly(ethylene-*alt*-propylene) (PEO−PEP)/ER blends, Bates et al.[4] concluded that the ER-swollen PEO blocks prior to the curing were repelled from the reactive ER matrix on a local level upon curing, presumably via a polymerization-induced phase separation. Therefore, the PEO was considered to be only partially miscible with the cured-ER phase. Mijovic[6] and Bates et al.[4] proposed two similar models to describe the phase separation in these blends. These models also predicted the existence

[†] Key Laboratory of Functional Polymer Materials for Adsorption and Separation, College of Chemistry.
[‡] College of Physics, Nankai University.
* To whom correspondence should be addressed: Tel +86-22-23507975; Fax +86-22-23507975; e-mail chenth@nankai.edu.cn.

10.1021/ma0505979 CCC: $30.25
Published on Web 05/26/2005

of an interphase region composed of PEO and partially cured ER. However, the amount of PEO expelled from the cured-ER network, the interphase thickness, and the dynamic properties of individual component have not been determined so far, and detailed information about these issues needs to be further elucidated.

Various techniques including differential scanning calorimetry (DSC), transmission electron microscopy (TEM), and small-angle X-ray scattering (SAXS) have been used to study the phase behavior and nanostructure of block copolymers and their blends.[4,7,10] Solid-state nuclear magnetic resonance (NMR) spectroscopy provides another powerful technique to study the structure and dynamics of crystalline polymers,[11] block copolymers,[12] polymer blends,[13] polymer membranes,[14] and polymer−inorganic hybrid materials.[15] NMR provides useful information about polymer microstructure due to its sensitivity to local chemical environments.[16] Furthermore, it can also be used to probe heterogeneous dynamics and monitor morphology changes. By measuring the time scale of proton spin diffusion, the length scales in nanoscopic heterogeneities from a few nanometers up to 100 nm and the interface between different microdomains can be determined.[17−19] Recently, Mirau et al. studied the structure and dynamics of PEO−PPO diblock copolymers in the bulk and their composites using the solid-state proton NMR technique, and the dynamics of PEO and PPO blocks, the interface, and domain size were successfully determined.[20] Solid-state NMR spectroscopy is expected to address many of the issues mention above in block copolymer/ER thermoset blends.[17,18,21] However, to the best of our knowledge, little NMR work was reported about the structure and dynamics for these block copolymer/ER thermoset blends.

In this paper, we report applications of NMR techniques to two ER/PEO−PPO−PEO thermoset blends containing 40 wt % triblock copolymer, denoted as ER/EO30 and ER/EO80, respectively. The compositions of these two samples were chosen to be the same as those used in the work of Guo et al.[7] We focus our attention on the heterogeneous dynamics, miscibility, microdomain structure, and interphase in these blends. To achieve these goals, ^{1}H MAS NMR was first used to detect the molecular mobility in these blends, and then detailed dynamic behavior and the miscibility of PEO block with the cured-ER network were obtained by ^{1}H dipolar filter experiments. 2D WISE NMR was used to gain information about the heterogeneous dynamics of individual components and to determine the extent of phase separation in the blends. The ^{1}H spin diffusion experiment was further employed to quantitatively determine the domain size, the long period, and the interphase thickness. On the basis of these studies, a tentative model with quantitatively structural information for the dynamic behavior and microdomain structure in these blends is proposed and compared with the previous models for the similar PEO-containing block copolymer/ER thermoset blends.

Experimental Section

Materials and Preparation of Samples. Materials and sample preparation in our work followed closely the procedure of Guo et al.[7] Two poly(ethylene glycol)-*block*-poly(propylene glycol)-*block*-poly(ethylene glycol) triblock copolymers (PEO−PPO−PEO), EO30 and EO80, with average molecular weight (M_n) of 5800 and 8400, were purchased from Aldrich Chemical Co., Inc. The calibrated contents of ethylene glycol (EO) in EO30 and EO80 by ^{1}H liquid-state NMR of the two samples in $CDCl_3$ were 36 and 79 wt %, respectively. The uncured epoxy resin (ER) was diglycidyl ether of bisphenol A (DGEBA) (Epikote 828, Shell Chemicals) with an epoxide equivalent weight of 185 g/equiv. 4,4′-Methylenedianiline (MDA) (Aldrich Chemical Co., Inc.) was used as curing agent. Two ER/PEO−PPO−PEO blends with 40 wt % PEO−PPO−PEO content, denoted as ER/EO30 and ER/EO80, were prepared according to the following procedure. 40 wt % EO30 or EO80 was first dissolved in DGEBA with continuous stirring at 120 °C. The curing agent MDA was then added to the mixture at 100 °C with continuous stirring until a homogeneous ternary mixture was obtained. MDA was used in stoichiometric epoxide/amine ratio. The mixture was then immediately poured into an aluminum pan, degassed at 90 °C in a vacuum, cured at 80 °C for 8 h, and then postcured successively at 150 °C for 2 h and 175 °C for 1 h. Finally, the samples were allowed to cool to room temperature for study.

Differential Scanning Calorimetry (DSC) Measurements. DSC experiments were performed on a NETZSCH DSC 204 differential scanning calorimeter in a dry nitrogen atmosphere. Samples of about 8 mg were placed in the DSC pan. All samples were first heated to 100 °C from −60 °C at a rate of 20 °C/min (first heating scan) and kept at that temperature for 2 min; subsequently, they were cooled at a rate of −20 °C/min to detect crystallization (cooling scan). Following the cooling scan, a second scan was conducted with the same heating rate as the first one. The midpoint of the slope change of the heat capacity plot of the second heating scan was taken as the glass transition temperature (T_g). The crystallization temperature (T_c) was taken as the minimum of the exothermic peak, whereas the melting temperature (T_m) was taken as the maximum of the endothermic peak.

Small-Angle X-ray Scattering (SAXS) Measurement. The SAXS experiment was performed at room temperature on a Bruker Nanostar small-angle X-ray scattering system consisting of Siemens X-ray generator operated at 40 kV; the distance between the samples and the detector was 646.0 mm. The plot of intensity vs scattering wave vector, q ($= 4\pi \sin(\theta/\lambda)$, where 2θ is the scattering angle and $\lambda = 0.154$ nm for Cu Kα radiation), was produced by circularly averaging two-dimensional scattering patterns. The long period, d_{long}, is inversely related to wave vector at the scattering peak, $d_{long} = 2\pi/q$.

NMR Experiments. NMR experiments were performed on a Varian UNITYplus NMR spectrometer at a proton frequency of 400 MHz. All experiments were carried out at room temperature (25 °C). In the liquid-state NMR experiments, all samples were dissolved in $CDCl_3$. In the solid-state NMR experiments, the samples were placed in a zirconia rotor, and a 5 mm CP/MAS probe was used. The magic angle spinning (MAS) speed was 4.5 kHz for 2D WISE (two-dimensional proton wide-line separation) and 8 kHz for dipolar filter experiments. The ^{1}H and ^{13}C chemical shifts were referenced to external TMS and HMB (hexamethylbenzene), respectively. Several solid-state NMR pulse sequences were used in this study.

(1) 2D WISE Experiments.[21,22] The WISE experiment correlates the ^{13}C CP/MAS spectrum (F2 dimension) with the proton wide-line spectrum (F1 dimension) due to ^{1}H−^{1}H and ^{13}C−^{1}H interactions. The pulse sequence is shown in Figure 1a; in this work, the mixing time (t_m) is set to zero without spin diffusion. Spectral widths of 40 and 100 kHz were used for the F2 and F1 dimensions, respectively, and typically 128 t_1 increments were used in the 2D WISE experiments. The 90° pulse length was typically 4.5 μs, the CP contact time was 400 μs to minimize the spin diffusion, and the recycle delay was 5 s.

(2) ^{1}H Dipolar Filter and Spin-Diffusion Experiment:[18,23,24] These experiments were used to measure chain dynamics and spin diffusion, respectively, as shown in Figure 1b,c. For ^{1}H dipolar filter experiments (Figure 1b), several cycles (N_{cycle}) of a 12-pulse dipolar filter sequence are first used to select the ^{1}H magnetization from the mobile phases which have longer transverse relaxation times than those of rigid phase. A 90° pulse is then used to detect the ^{1}H signals. Lorentzian lines

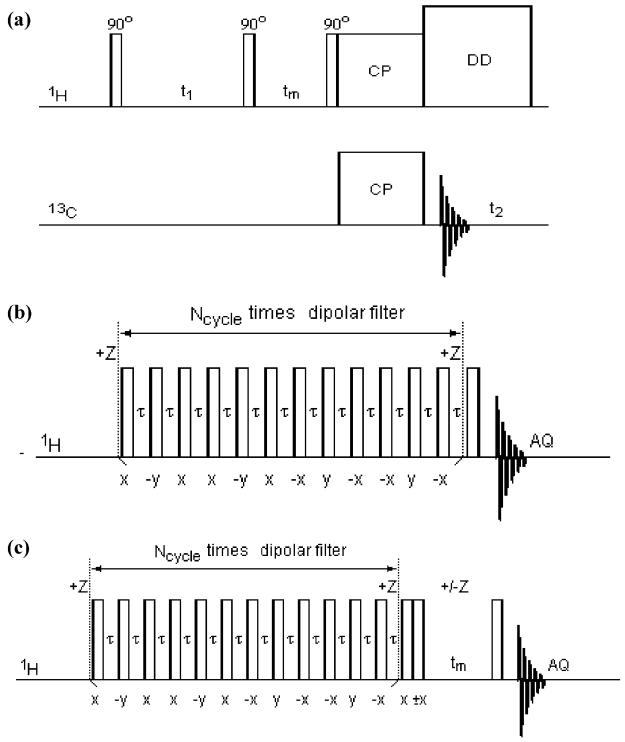

Figure 1. (a) Pulse sequence for the WISE experiment,[13] including an optional mixing time t_m. CP and DD stand for cross-polarization and dipolar decupling, respectively. (b) Pulse sequence with a 12-pulse dipolar filter for ^{1}H dipolar filter experiment. (c) ^{1}H spin diffusion measurement with only ^{1}H magnetization of the mobile phases selected.

were used in the deconvolution of the ^{1}H dipolar filter spectrum. For the ^{1}H spin-diffusion experiment (Figure 1c), the first step is also several cycles of a 12-pulse dipolar filter. A pair of 90° pulses was then placed immediately after the dipolar filter with 0° and 180° phase-cycled in order to eliminate the effect of T_1 relaxation during the mixing period. The following step is a "mixing" period (t_m) in which the remaining proton magnetization diffuses to neighboring spins. The final step is the direct ^{1}H detection. The domain sizes can be determined using proton spin diffusion when the polarization gradient is relaxed. The effects of T_1 relaxation were removed from the spin-diffusion decay curve by making use of T_1 values, which were independently measured using the standard inversion−recovery sequence with a recycle delay of $3-5T_1$. Under MAS conditions, the rotor period was carefully adjusted so that it is not an integral multiple of the filter cycle. The 90° pulse length was 3.2 μs, and the interpulse spacing of τ was typically 8−15 μs. Since the spin-diffusion coefficients can be strongly affected by MAS,[20,21,25] all spin-diffusion experiments in this work were performed under static conditions.

Results and Discussion

Characterization of PEO Crystallinity by DSC and Microphase Structure by SAXS Experiments. The phase behavior, crystallization of PEO, and hierarchical nanostructures in the 60/40 (w/w) MDA-cured ER/EO30 and ER/EO80 blends have been characterized in detail by DSC, SAXS, TEM, and AFM techniques in previous studies.[7] To make a direct comparison between our NMR results and the results from Guo et al.,[7] all the samples were first examined using DSC in order to check the samples' consistency between the two works. Figure 2 shows the DSC traces of the second heating scan and the cooling scan of EO80, EO30, ER/EO80, ER/EO30, and MDA-cured ER. All these traces are in

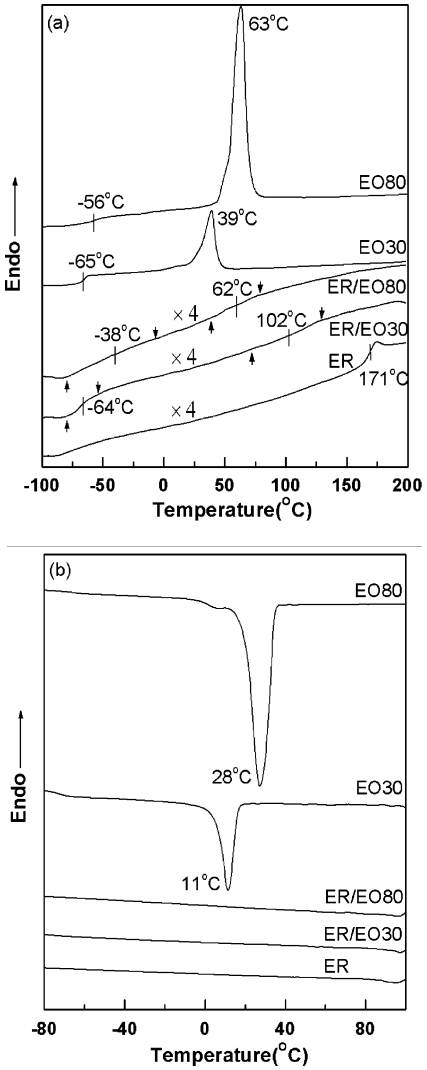

Figure 2. DSC traces of EO80, EO30, ER/EO80, ER/EO30, and MDA-cured ER. (a) The second heating scan and (b) the cooling scan. The heating traces in (a) were enlarged 4 times for ER/EO30, ER/EO80, and MDA-cured ER. The arrow pointing upward denotes the temperature at which the transition begins, the arrow pointing downward denotes the temperature at which the transition ends, and the line (|) denotes the midpoint (T_g) of the transition.

agreement with those reported in the previous work, [7] while only the T_m (39 °C) and T_c (11 °C) of EO30 show some difference with those reported at 33 and −27 °C, respectively. ^{1}H liquid-state NMR indicated that the EO content was 36 wt % in our EO30 sample, which was slightly higher than 30 wt % provided by the manufacturer. In the DSC traces of the two blends, only in ER/EO30 the T_g of the copolymer at −64 °C was clearly visible, while the other glass transitions were not well resolved and the T_gs (at around 102 °C for ER/EO30, −38 and 62 °C for ER/EO80) could only be estimated by taking the midpoint of the slope change of the heat capacity plot of the second heating scan. The DSC results clearly indicate that the semicrystalline PEO in EO80 and EO30 changed to amorphous forms in the ER/EO80 and ER/EO30 blends, implying the formation of PEO crystalline domains in these two blends was inhibited.

To evaluate the influence of EO30 on themicrophase structure of the ER/EO30 blend, we further performed the SAXS measurement, as shown in Figure 3. A

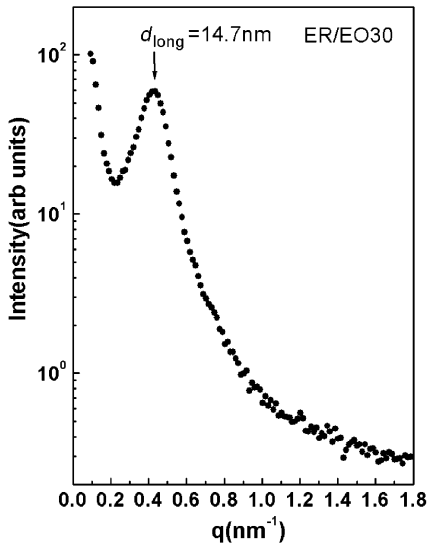

Figure 3. SAXS pattern of MDA-cured ER/EO30 blend.

scattering peak is clearly observed corresponding to a long spacing of 14.7 nm in real space, which is in good agreement with the reported value of 15.1 nm for the same ER/EO30 sample.[7] This implies that the microdomain structure of ER/EO30 blend used in this work is similar to that in the reported work of ref 7.

Dynamics and Phase Behavior Determined by ^{1}H MAS NMR. It is well-known that the line width of the ^{1}H line reflects the nature of the dipolar interaction between the protons and thus can be used to monitor the dynamic behavior of polymer chains.[21,26] For glass and crystalline polymers, the chain segments are rigid, and the dipolar couplings of protons for these polymers are generally on the order of 30−50 kHz. For polymers above T_g, the dipolar couplings are partially averaged by chain motion, and a high-resolution spectrum can be obtained with moderate magic angle spinning.[27] Since the glass transition temperatures for amorphous PEO and PPO (about −70 and −75 °C)[28] are well below the ambient temperature, the signal of these mobile segments could be effectively narrowed with fast MAS. In our ^{1}H MAS NMR experiments, MAS speed of 8 kHz was adopted, which is fast enough for line narrowing for amorphous PEO and PPO polymers above T_g but is insufficient to narrow the lines for the cross-linked ER network and PEO crystalline region. If the copolymers were completely dissolved in the rigid cross-linked ER network, all the ^{1}H signals of the copolymer would be remarkably broadened. If they were phase separated, narrow lines arising from amorphous PEO and PPO could be obtained under moderate MAS conditions.

The dynamic difference between the mobile and rigid components is clearly visible in the static ^{1}H single-pulse spectra, as shown in Figure 4. The broad hump (∼40 kHz fwhm) at the bottom of the spectra is assigned to cross-linked ER network, and the relative narrow peaks (2−6 kHz fwhm) at the center of the spectra are assigned to PEO−PPO−PEO copolymers. Because the signals from the rigid cross-linked ER network with strong dipolar interactions in ER/EO30 and ER/EO80 blends are very broad in Figure 4, ^{1}H static NMR clearly indicates that phase separation occurred in the two blends because of the remarkable molecular mobility differences between the cross-linked ER and the copolymers.

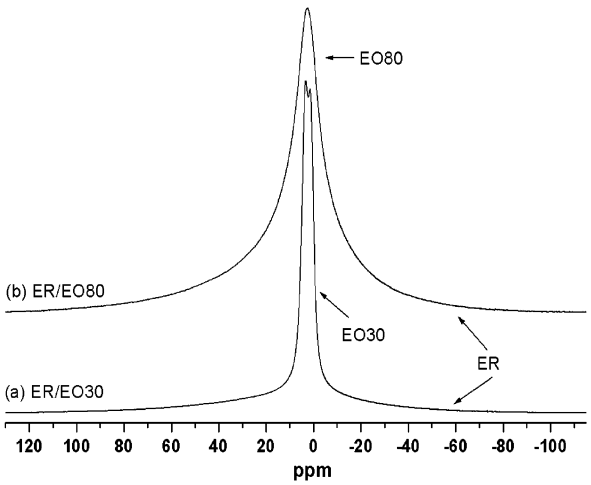

Figure 4. ^{1}H static NMR spectra of (a) ER/EO30 and (b) ER/EO80.

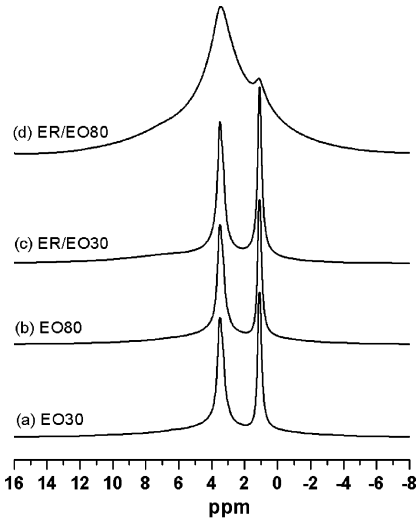

Figure 5. Expanded ^{1}H MAS NMR spectrum of (a) EO30, (b) EO80, (c) ER/EO30, and (d) ER/EO80 at 8 kHz MAS.

Figure 5 shows the expanded ^{1}H MAS NMR spectra for all samples acquired with 8 kHz magic angle spinning. It is clear that resolutions of the spectra are improved. The signal at around 3.5 ppm was assigned to the overlapped peaks arising from the methylene protons of PEO and the methine and methylene protons of PPO, and the signal at 1.1 ppm was assigned to methyl protons of PPO block.

For EO30 and EO80 samples, Figure 5a,b shows that the PPO block is relatively mobile and exhibits narrowed lines. If all of the protons from PEO and PPO had been mobile enough to be completely observed, the expected peak intensity ratios for the peaks at 3.5 and 1.1 ppm would be 2.0:1 and 8.3:1 for EO30 and EO80, respectively, which are the same as the value determined from the ^{1}H liquid-state NMR spectra of EO30 and EO80 in $CDCl_3$. However, the obtained intensity ratios from ^{1}H MAS spectra were only around 1.4:1 and 1.2:1 for EO30 and EO80, respectively. Since a 1:1 intensity ratio is expected from the PPO block alone, this implies that a significant fraction of the intensity at 3.5 ppm is missing from the spectra. We can reasonably infer that this should be due to a large fraction of the PEO in rigid crystalline region, and most of the signals for the semicrystalline PEO block are too broad to be observed. The observed peak at 3.5 ppm is

therefore due to the methine and methylene protons of PPO and amorphous PEO methylene protons. The conclusion that the PEO blocks in EO30 and EO80 are partially crystalline is consistent with the DSC experiments displayed in Figure 2a, showing sharp melting transitions at about 39 and 63 °C, respectively.

For the ER/EO30 blend (Figure 5c), the relatively sharp peaks at 3.5 and 1.1 ppm could also be assigned to the mobile PEO and PPO blocks. For the ER/EO80 blend (Figure 5d), it is interesting to see that the peak at 3.5 ppm became obviously high and broad, and this will be discussed in detail in the following ^{1}H dipolar filter experiments.

Heterogeneous Dynamics and Miscibility Determined by Proton Dipolar Filter. Proton dipolar filter experiment shown in Figure 1b can provide detailed information about the structure, heterogeneous dynamics, and miscibility in polymer blends.[20,23,24] For polymer blends composed of rigid and mobile phases, with the increasing of the dipolar filter strength, the ^{1}H magnetization from the rigid phase will be suppressed due to its shorter transverse relaxation time than that of the mobile phase. The peak intensity as a function of the dipolar filter strength provides useful information about the dynamics heterogeneity. In addition, subtle structure information can also be obtained because the resolution of the ^{1}H MAS spectrum will be further improved due to the suppression of the broad peaks arising from protons in the rigid region.

Figure 6 shows the effect of increasing dipolar filter strength, i.e., the cycle number of the 12-pulse sequence (N_{cycle}), on the spectra of ER/EO30 and ER/EO80 samples under 8 kHz MAS and a delay time $\tau = 8$ μs. In Figure 6a for ER/EO30, the MAS spectrum without dipolar filter ($N_{cycle} = 0$) exhibits both broad and narrow components. The broad component at the bottom of the spectrum was suppressed by using one cycle of the 12-pulse dipolar filter, indicating that the dipolar interaction of this component is stronger than the mobile component. On the other hand, the line width of this broad component was far less than that of the rigid ER phase (~40 kHz fwhm). Therefore, it is reasonably to assign this broad signal in Figure 6a to the interphase between the rigid and mobile phases, denoted as "immobilized". A strong dipolar filter with $N_{cycle} > 7$ produces relatively small changes in either the intensity ratio or the line width of the remaining signals. Because of their weak dipolar interaction, the remaining signals after the strong dipolar filter ($N_{cycle} > 7$) could be attributed to the mobile copolymer phase. The intensity ratio of the peaks at 3.5 and 1.1 ppm after the strong dipolar filter is approximately 1.3:1. Since the intensity ratio of the peaks at 3.5 and 1.1 ppm for PPO alone is 1:1, the fraction of mobile PEO was then calculated to be about 30% of total PEO, which implies that about 70% of total PEO is immobilized and exhibits broad lines. These immobilized PEO should be in close proximity to or intimately mixed with the cured-ER phase.

In Figure 6b for the ER/EO80 blend, a significant decrease in the signal intensity for the peak at 3.5 ppm was found with increasing dipolar filter strength from $N_{cycle} = 1-9$, indicating that the broad hump (in the spectra when $N_{cycle} = 0$) could result from the immobilized PEO protons as well. A further increase of N_{cycle} up to 11 produces relatively small changes in either the intensity ratio or the line width of the remaining signals corresponding to the mobile phase of

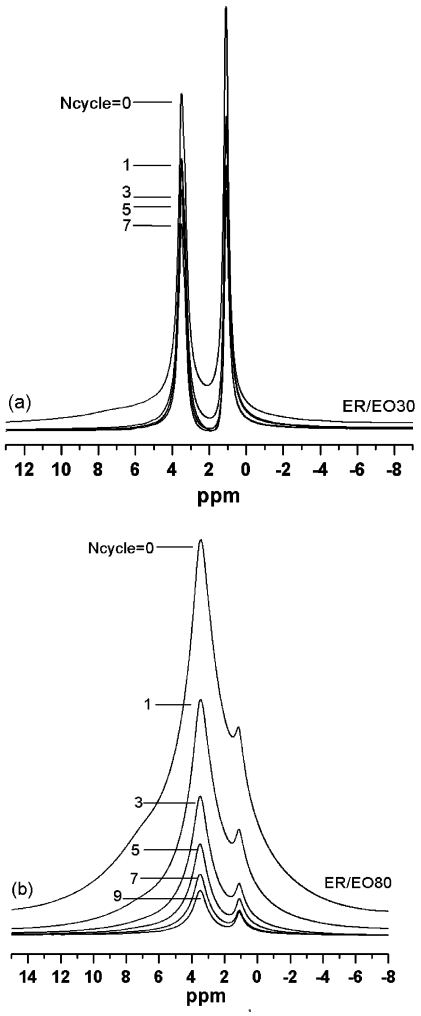

Figure 6. Effect of dipolar filter strength on the ^{1}H MAS spectra for (a) ER/EO30 and (b) ER/EO80 at 8 kHz MAS. The filter strength is increased by increasing N_{cycle} in dipolar filter pulse sequence as shown in Figure 1b.

PEO and PPO. The ^{1}H MAS NMR spectrum with a strong dipolar filter ($N_{cycle} = 9$) was deconvoluted with two overlapping Lorentzian lines, and the calculated intensity ratio of the peaks at 3.5 and 1.1 ppm was approximately 4.0:1. Since the intensity ratio of the peaks at 3.5 and 1.1 ppm for PPO alone was 1:1, the mobile fraction of total PEO at 3.5 ppm was then calculated to be around 41%, which implies that about 59% of total PEO is in close proximity to or is mixed with the cured-ER phase. These observations of ER/EO30 and ER/EO80 confirm that the PEO blocks are only partially miscible with the cured-ER network. The line widths of ER/EO80 were obviously broader than those of ER/EO30 under strong filter strength, indicating that the chain motion of the mobile phase (PPO and PEO) in ER/EO80 was more restricted than in ER/EO30. The measured higher T_g (−38 °C) of PPO in ER/EO80 ($T_g = -64$ °C in ER/EO30) (see Figure 2a) is consistent with this conclusion.

It should be pointed out that in the above analysis of the immobilized PEO fraction in these blends the possible different relaxation behaviors of the CH_2 groups in PEO and PPO were not taken into account. For ER/EO30, due to the relatively strong signal left after the dipolar filtering, the fraction value obtained may not be seriously affected by the relaxation effect. For ER/EO80, since not much of the initial signals were left

after extensive dipolar filtering, the above estimation of immobilized PEO fraction may be influenced by the assumption that mobile CH_2 groups in PEO and PPO relax equally under the dipolar filter. However, the immobilized PEO fractions could also be obtained by spin diffusion experiments without assuming similar relaxation behavior of CH_2 groups in PEO and PPO, and the results from spin diffusion (see below) are rather supportive to those from the dipolar filter experiments.

In Figure 6, we can also observe a weak shoulder at about 7 ppm for ER/EO30 and ER/EO80 without dipolar filter ($N_{cycle} = 0$). This weak signal was not as broadened as that of the rigid cross-linked ER network and could be completely suppressed by gradually increasing dipolar filter strength. We suggest that this signal might be attributed to the "mobilized" partially cured ER. These partially cured ER was intimately mixed with the immobilized amorphous PEO blocks mentioned above to form the interphase region. This observation also supports the prediction of a "middle layer" containing PEO and partially cured ER in the PEO−PPO/ER blend, as suggested by Mijovic et al.[6] A quantitative measurement of the interphase was performed in the later proton spin diffusion experiments, and as discussed later in this work, the spin-diffusion results were not affected by this 7 ppm partially cured-ER signal (see below).

Correlation of Mobility and Domain Structure by 2D WISE Spectroscopy. Because of the narrow chemical shift range of ^1H, the peaks at 3.5 ppm arising from PEO and PPO overlapped as shown in Figure 6. To achieve a better understanding of the detailed dynamics and the phase behavior in the ER/EO30 and ER/EO80 blends, we employed a 2D WISE NMR experiment that has been widely used for the determination of heterogeneous dynamics in solid polymers.[13b,18,21,22] WISE is useful for the characterization of polymers with complex morphology that include hard and soft domains, such as polymer blends and block copolymers. Different domains are distinguished by the ^1H wide-line spectrum, broad if rigid and narrow if mobile. At the same time, the observed ^{13}C chemical shifts indicate the segmental composition of the regions. This method can be used to determine the degree of phase separation qualitatively, and it allows one to characterize whether there is an extended interphase between the two phases in phase-separated blends. In addition, the obtained line widths of individual components from 2D WISE spectroscopy can be used to calculate the spin-diffusion coefficient for the determination of the domain size (see the following section).

Parts a and b of Figure 7 display the $^{13}C-^1H$ WISE spectra of ER/EO30 and ER/EO80, respectively, which clearly show distinctly different mobility for the individual component and confirm the existence of phase separation in the blends. The appearance of three strong and narrow peaks of PPO at 72.0, 74.0, and 16.5 ppm on ^{13}C dimension implies that the PPO blocks are mobile and segregated from the rigid ER matrix, whereas the ER matrix which exhibits remarkably broadened NMR lines. From the slice projection of PEO peak at 70 ppm (Figure 7c,d), it was found that the PEO blocks exhibited both narrow and broader lines corresponding to mobile and immobilized components, respectively, providing an independent evidence supporting the assignment of the ^1H dipolar filter experiments. This result confirms again that the PEO blocks are only partially miscible with the cured-ER network, and the narrow component could be assigned to the mobile PEO blocks segregated from the cured-ER matrix. Since PEO was completely amorphous in this blend from the DSC results, it is reasonable to assume that the broad component should be attributed to the immobilized PEO in the interphase region. The WISE NMR results are in good agreement with those obtained by ^1H NMR experiments. We also noticed that no obvious "mobilized" ER signal (at 7 ppm in Figure 6) was observed in the WISE spectra. This could be due to its intermediate mobility, inefficient cross-polarization, and/or very short $T_{1\rho}$ of the signal.

Characterization of the Interphase by Proton Spin Diffusion. Interphase of polymer blends has been an attractive subject in the past years.[29,30] In general, an ideal structure with complete phase separation in a blend cannot be obtained. Instead, the interfacial width is finite and an interphase between the phases is formed. Understanding the nanoscale interphase property is crucial because it plays an important role in controlling the final structure and property of the blends. Because of the extremely small volume fraction of interphases in a typical polymer blend, experimental determination of interphase property has been a challenging subject. It is important to have a method which enables a quantitatively determination of the fine structures of the interface on the scale of 0.1−20 nm. TEM and X-ray scattering techniques have been successfully applied to detect the existence of an interfacial region.[30] The ^1H spin-diffusion NMR experiment is another powerful method, which not only allows one to estimate the interphase thickness but also provides detailed information about structures and composition in interfacial regions.[18,31]

Detailed treatments of ^1H spin diffusion experiments are available in the literature. For convenience of our discussion, we briefly review the main features as proposed by Spiess et al.[18,21] and only consider the polymer blend composed of rigid and mobile components as well as immobilized interphase. In the following discussion, the word "immobilized" polymer means that the polymer is in the regime of intermediate mobility between "rigid" and "mobile".

In spin-diffusion experiments, the magnetization of one of the polymer fraction has to be suppressed, while the other is selected to be conserved. This can be performed by using dipolar filter sequence as shown in Figure 1c. Because of different T_2 relaxation behavior during the dipolar filtering, the signals arising from the rigid region can be suppressed. Thus, at the start of the mixing period, only protons from relative mobile region have a net magnetization depending on the filter strength. During the mixing time, this magnetization is transferred by spin diffusion. Since the rate of spin diffusion is related to internuclear distance and the extent of molecular mobility, such experiments allow the length scales in the blend to be determined. In general, the interphase in a two-component system is the region of gradual change in structure and molecular mobility between different phases. In the case of mobility gradient arising from gradient of composition, dipolar coupling also exhibits a gradual change between the values of the pure phases. With increasing dipolar filter strength in the spin-diffusion experiments, regions with different mobilities due to different transverse relaxation times T_2 can be selected. This allows one to obtain information about the different immobilized parts in the interphase region.

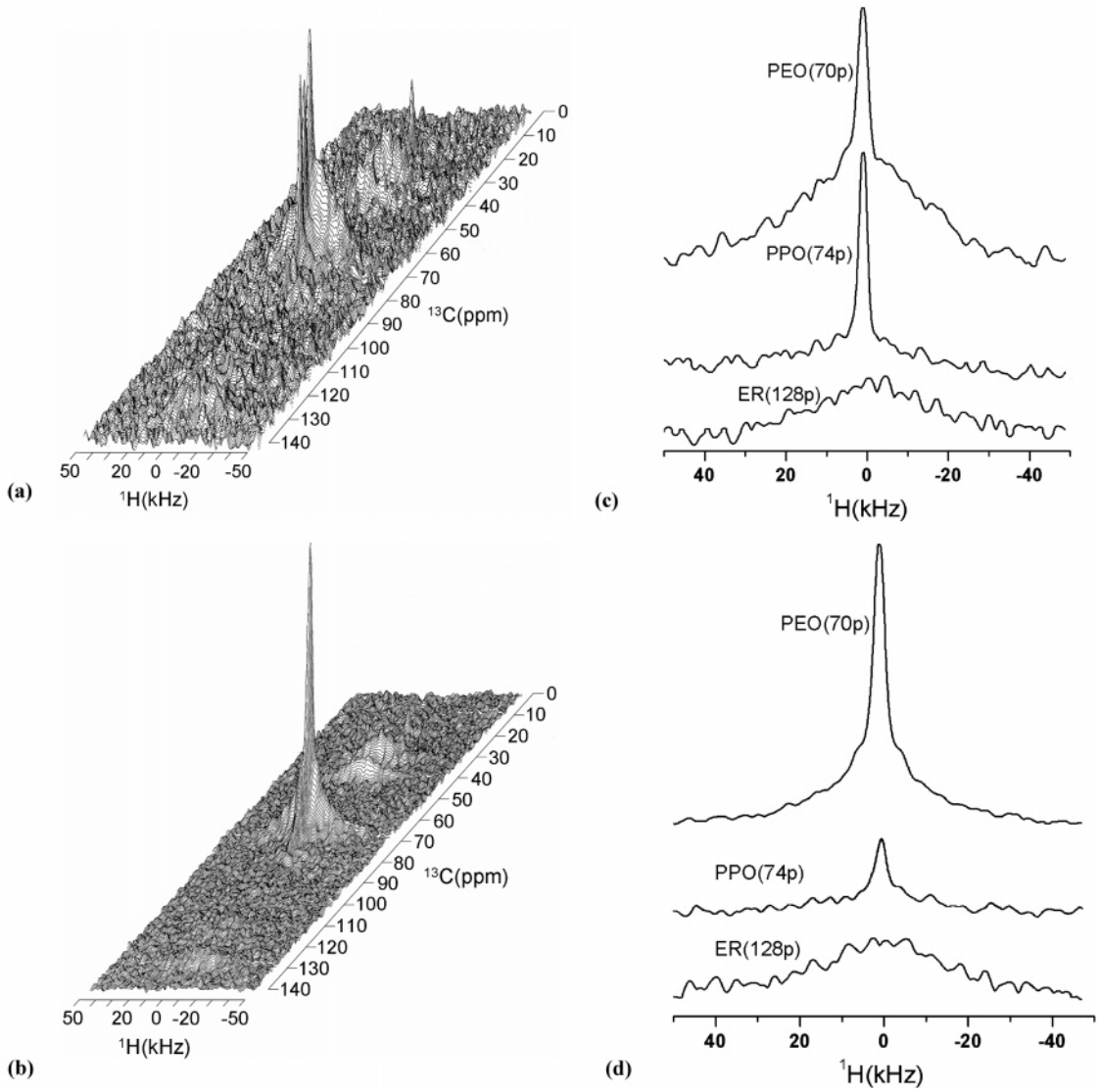

Figure 7. 2D $^{13}C-^{1}H$ WISE spectra for (a) ER/EO30, (b) ER/EO80, and corresponding ^{1}H projection of (c) ER/EO30 and (d) ER/EO80.

Figure 8a shows schematic spin-diffusion curves after the application of different dipolar filter strength for a blend containing a rigid (black) and a mobile (white) component. The interphase (gray) with mobility gradient is also illustrated. The signal intensity I of retained the ^{1}H signals is plotted as a function of mixing time $t_m^{1/2}$. The curves are normalized with respect to the intensity at $t_m = 0$, I_0. Because the experimental spin-diffusion curves shown later are T_1 corrected, the T_1 effect is neglected in the schemes. The characteristic mixing time of spin diffusion, $t_m^{s,0}$,[23] detected at certain filter strength reflects the initial slope of the curve (dot line) and depends directly on the domain size (will be discussed later). The end (plateau) value of the curve contains important information about the interphase. For certain filter strength, the end value corresponds to the selected fraction of protons in the blend, and it decreases with increasing filter strength. For the ER/EO30 and ER/EO80 in this study, the contributions from the protons in the rigid cured-ER region are too broad to be observed. In the case of weak dipolar filters, the mobile phase and the interphase with the partially cured (mobilized) ER could be selected, and the end value might be higher than expected from the stoichiometric proton ratio (curve A). With a strong filter, only the mobile phase near the interfacial region is selected. The end value is lower than expected from the stoichiometric proton ratio (curve B). The selected mobile component can be directly determined from the end value of the spin-diffusion curve. The difference of the measured end value to the expected stoichiometric one is the amount of immobilized fraction in the interphase region.[18] In the case of ideal phase separation, only the separated mobile phase is selected; the end value should directly reflect the proton ratio of the components denoted as the stoichiometric end value, as shown in Figure 8a.

A detailed analysis for the evolution of the selected fraction (end value) with increasing dipolar filter is very important to quantitatively determine the interphase thickness and distinguish blends with different phase separation. On the basis of the work of Spiess et al.,[18] we now propose a new and useful representation for spin-diffusion experimental results used to determine the interphase thickness. Figure 8b shows the schematic curve of the selected fraction (end value) in a spin-diffusion experiment with increasing filter strength (N_{cycle}). Although this curve is similar to the spin-diffusion curve shown in Figure 8a, it has different meaning. The significance of the equilibrium selected

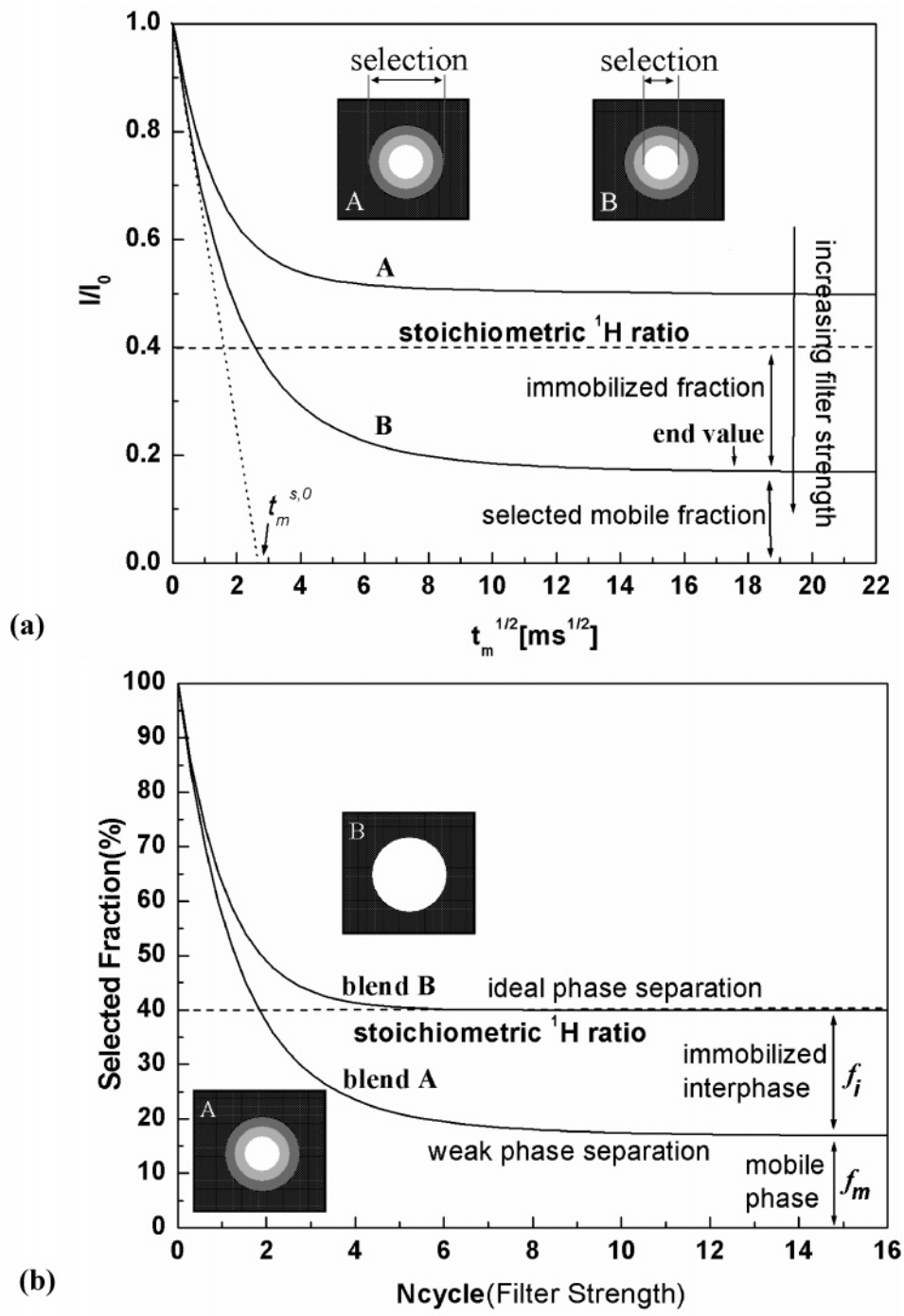

Figure 8. (a) Schematic spin-diffusion curves showing the significance of the end (plateau) value and the effect of different dipolar filter strength. The end value of the spin-diffusion curve represents the selected fraction of protons in the blend. The suppressed rigid fraction can be calculated from (1 − selected mobile fraction). The immobilized fraction represents the difference between the stoichiometric ratio and the selected mobile fraction. With increasing filter strength the end value decreases. A weak filter selects both the mobile phase and the immobilized interphase; a strong filter selects only the mobile phase. The description of curves A and B is given in the text. (b) Schematic curve of the selected fraction (end value) in spin-diffusion experiment with increasing filter strength (N_{cycle}). The interphase as well as the extent of phase separation in blends containing rigid and mobile components can be determined from the curves.

fraction at stronger filter strength (denoted as "final value"), e.g., $N_{cycle} > 10$, represents the fraction of the mobile phase. This final value is very important to quantitatively determine the immobilized component and its fraction in interphase region. In Figure 8b, two blends with different interphase can be well distinguished, and the fraction of the interphase in the blend can be quantitatively determined. For blend A with weak phase separation, the final value must be lower than that expected from the stoichiometric ratio, indicating the presence of a immobilized interphase; the fraction of the interphase protons can be determined from the difference of the stoichiometric ratio with the final value. For blend B with ideal phase separation, the final value should be the same as the stoichiometric ratio that indicates the absence of the interphase. From the above discussions, we can conclude that the spin-diffusion experiment is a powerful and convenient method to elucidate the structure and dynamics of the interphase in blends.

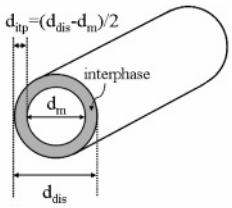

Figure 9. Schematic diagram of the relationship of d_m, d_{dis}, and d_{itp} for a cylindrical ($p = 2$) domain. Here, the length of the cylinder is considered to be far greater than d_{dis}.

Because the proton fraction of the interphase and the mobile phase, f_i and f_m, can be quantitatively determined from the curves shown in Figure 8b, the thickness of the interphase for blend A in Figure 8b, d_{itp}, can be directly estimated. Assuming the proton densities in the mobile phase and interphase are nearly homogeneous, the volume of the selected mobile phase V_m can be approximately written as

$$V_m = \frac{f_m}{f_i + f_m} V_{dis} \tag{1}$$

where V_{dis} is defined as the volume of the dispersed phase including both the interphase and the mobile phase. For a given morphology, the volume V can be written as

$$V = kd^p \tag{2}$$

where p represents the dimension, and its value depends on the morphology: $p = 1$ for lamellar, 2 for cylinder with the length of the cylinder considered to be far greater than its diameter, and 3 for discrete phase, such as spheres in a matrix; d is the domain size, i.e., the thickness for $p = 1$ and the diameter for $p = 2$ or 3. Parameter k represents the section area of the lamellar for $p = 1$, $\pi/4 \times$ length of the cylinder for $p = 2$, and constant $\pi/6$ for $p = 3$. The k factors are the same in V_m and V_{dis}. In the following discussions, we define d_m and d_{dis} to be the domain size of the mobile and dispersed phase, respectively. Figure 9 shows the schematic diagram of the relationship of d_m, d_{dis}, and d_{itp} for $p = 2$.

Combine eqs 1 and 2, we have

$$d_m = \sqrt[p]{\frac{f_m}{f_i + f_m}}\, d_{dis} \tag{3}$$

Thus, the interphase thickness, d_{itp}, can be written as

$$d_{itp} = (d_{dis} - d_m)/2 = \frac{1}{2}\left(1 - \sqrt[p]{\frac{f_m}{f_i + f_m}}\right) d_{dis} \tag{4}$$

By using a suitable filter strength to select the proton fraction at the stoichiometric proton ratio, d_{dis}, the size of dispersed domain including both the mobile phase and immobilized interphase can be determined using the initial slop of the spin-diffusion curve. Then the interphase thickness d_{itp} can be directly determined from eq 4, i.e., on the basis of f_i and f_m which could be determined from dipolar filter experiments (Figure 10, see blow). The method used here to estimate d_{itp} may only be suitable for the blend with a large molecular mobility contrast in the different phases.

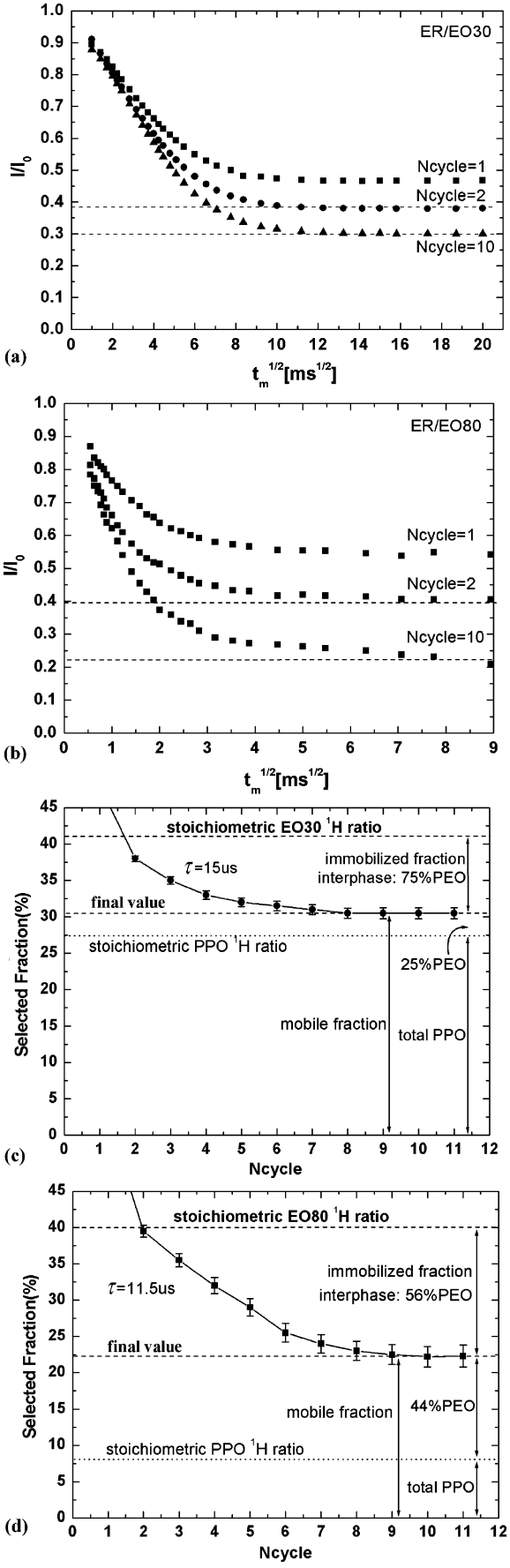

Figure 10. Static spin-diffusion curve for (a) ER/EO30 and (b) ER/EO80 at different dipolar filter strengths (N_{cycle}). Selected fraction as the function of filter strength (N_{cycle}) for (c) ER/EO30 and (d) ER/EO80.

Table 1. Proton Fractions of EO30 and EO80 in ER/EO30 and ER/EO80 Blends as Well as the Proton Fractions of PPO in EO30 and EO80 Determined by ^{1}H Liquid-State NMR in $CDCl_3$

samples	ER/EO30	ER/EO80	EO30	EO80
proton fraction of copolymer (stoichiometric proton ratio) (%)	41.4	39.9		
proton fraction of PPO (%)	27.5	8.5	66.4	21.4

Before carrying out the spin-diffusion experiments, the proton ratio of the copolymers in the ER/EO30 and ER/EO80 blends should be determined. Element analysis and ^{1}H high-speed MAS NMR had been used to determine the stoichiometric proton ratio of polymers in previous report by Spiess et al.[32] In this work, we directly used ^{1}H liquid NMR to determine the stoichiometric proton ratio of the samples before curing. Table 1 lists all the measured stoichiometric proton ratios of the block copolymers used in the ER/EO30 and ER/EO80 blends, together with the proton fractions of PPO in EO30 and EO80 copolymers. These parameters will be used to determine the fraction of the PEO in the mobile phase.

The static spin-diffusion spectra for the blends were obtained with the pulse sequence shown in Figure 1c with different mixing time t_m. Figure 10a shows the spin-diffusion curves with increasing dipolar filter strength for ER/EO30. The evaluation of spin-diffusion curve was performed using a strategy proposed by Spiess et al.[23] For small mixing times (1 ms < t_m < 20 ms) the spin-diffusion curves possess a linear slope, and the intensity at $t_m = 0$ can be reliably extrapolated from the initial data points of the spin diffusion curve. To eliminate the effect of spin−lattice relaxation on the measurement of spin diffusion, the intensity data were corrected for spin−lattice relaxation (T_1) using the multiplicative factor $\exp(+t_m/T_1)$.[21] The two dashed lines denote the different end (plateau) values, i.e., the selected fraction, of the spin diffusion curves with different dipolar filter strengths. Figure 10c shows the selected fraction in spin-diffusion experiments for ER/EO30 blend with different filter strength (N_{cycle}). The final value (30.9% at $N_{cycle} > 8$) is obviously lower than that expected from the stoichiometric proton ratio (41.4%), indicating a weak phase separation and the existence of a large interphase region. Comparing this figure with Figure 8b, we obtain that about 75% (f_i) immobilized PEO is in the interphase region which were intimately mixed with ER, while the mobile components (25%) of the PEO and all of the PPO (f_m) are expelled from the cured-ER network.

Figure 10b shows selected fractions in the spin diffusion experiments for the ER/EO80 blend with different filter strengths. The final value ($N_{cycle} > 9$) is lower than that expected from the stoichiometric proton ratio (39.9%). Again, this indicates a weak phase separation and the existence of a large interphase region. Quantitatively, about 56% (f_i) immobilized PEO is in the interphase region, while the mobile PEO components (44%) and all PPO (f_m) are repelled from the cured-ER network.

The above quantitative results from spin-diffusion measurements of ER/EO30 and ER/EO80 confirm again that the PEO blocks are not completely dissolved in the cured-ER network. It also indicates that more PEO blocks were repelled from the ER phase in ER/EO80 as compared with ER/EO30, although the weight fraction of PEO increased from 36% in EO30 to 79% in EO80 and PEO has a good miscibility with ER before curing. These spin-diffusion results are in good agreement with those obtained from the ^{1}H dipolar filter experiments discussed earlier on, which implies that the dynamics of the mobile EO and PO within the same domain may not be that different. Compared with the dipolar filter method, the spin-diffusion method is more general, and it can provide more accurate results for the estimation of the immobilized PEO in the blends. It should also be pointed out that the broad "mobilized" ER signal in the 6−8 ppm region could be significantly suppressed in dipolar filter experiments when $N_{cycle} = 1$ for ER/EO30 and $N_{cycle} = 2$ for ER/EO80; thus, the spin-diffusion results were not affected by this broad ER signal.

Although the proton density of PEO is slightly different from that of PPO in EO30 and EO80 copolymers, as an estimation, we can use eq 4 to determine the interphase thickness (d_{itp}) in the two blends, and we obtain $d_{itp} = 0.07d_{dis}$ and $0.13d_{dis}$ for ER/EO30 and ER/EO80, respectively. In the next section, the value of domain size d_{dis} and interphase thickness d_{itp} will be determined by spin-diffusion experiments, leading to a quantitative estimate of the interphase thickness.

Determination of Domain Sizes by Spin Diffusion. The presence of significant heterogeneous dynamics revealed by dipolar filter and 2D WISE experiments suggests the possibility of determining the domain size in these phase-separated mixtures by measuring the rate of proton spin diffusion following the dipolar filter in spin-diffusion experiment.[21] In contrast to other techniques, spin diffusion is particularly suited for the characterization of small domains, nanoheterogeneities on length scales of a few nanometers, where other methods often fail owing to limitations in resolution or contrast. The domain size of the dispersed phase A in the two-phase A/B mixture, d_{dis}, can be determined[33] by the following equation[17,21]

$$d_{dis} = \epsilon\sqrt{4D_{eff}t_m^{s,0}/\pi} \tag{5}$$

where ϵ represents the dimension, and its value depends on the morphology and is 1 for lamellar, 2 for cylinder-like, and 3 for discrete phase, such as spheres in a matrix. $t_m^{s,0}$ is the characteristic mixing time of spin diffusion introduced by Spiess et al.,[23] and it can be determined by the intercept of the extrapolated linear initial decay with the X-axis in the spin-diffusion curve, as shown in Figure 8a. The effective spin-diffusion coefficient D_{eff} is defined according to the following equation

$$\sqrt{D_{eff}} = \frac{2\sqrt{D_A D_B}}{(\rho_A^H/\rho_B^H)\sqrt{D_A} + \sqrt{D_B}} \tag{6}$$

where ρ_A^H and ρ_B^H are proton densities.

Different methods were proposed to estimate the diffusion coefficients for mobile and rigid phase.[23,33,34] The diffusion coefficient of the mobile phase, denoted as D_A here, can be calculated from the following equation, which is valid for the Lorentzian line shape:[34]

$$D_A = \frac{1}{6}\langle r^2\rangle\,[\alpha\Delta\nu_{1/2}^A]^{1/2} \tag{7}$$

where $\langle r^2\rangle$ is the mean-square distance between the nearest spins (typically of the order of 0.04−0.06 nm^2

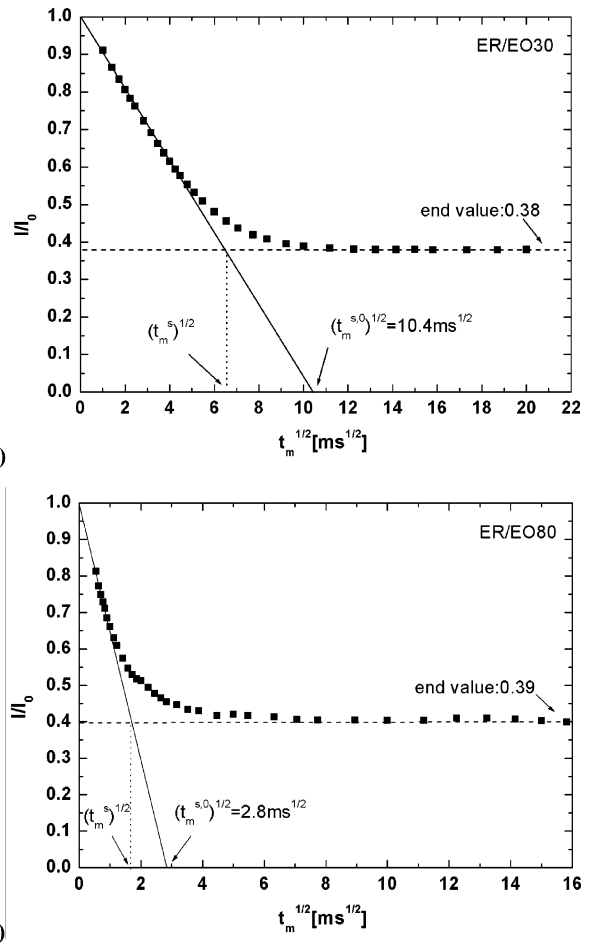

Figure 11. Spin-diffusion curves, plotted as the normalized intensity I/I_0 against the square root of the mixing time t_m, for (a) ER/EO30, and (b) ER/EO80 blends with $N_{cycle} = 2$. The extrapolated value $t_m^{s,0}$ is estimated and denoted in the figure. The value t_m^s used in ref 21 is also denoted.

in polymer), α is a cutoff parameter which is defined such that the absorption spectrum intensity is zero for the frequency range $|\Delta\omega| > \alpha$, and $\Delta\nu_{1/2}^{A}$ is the line width of proton wide-line signals obtained by 2D WISE experiment of selected mobile phase A.

The diffusion coefficient of the rigid phase can be calculated from the following equation that is valid for the Gaussian line shape:[34]

$$D_B = \frac{1}{12}\sqrt{\frac{\pi}{2\ln 2}}\langle r^2\rangle \Delta\nu_{1/2}^{B} \tag{8}$$

where $\Delta\nu_{1/2}^{B}$ is the line width of proton wide-line signals obtained by 2D WISE experiment of rigid phase B. On the basis of the geometrical considerations for different morphologies, the length of the long period, d_{long}, can be calculated.[33]

For a two-dimensional (cylindrical) morphology, d_{dis} is the rod diameter and d_{long} is the rod spacing, which can be written as

$$d_{long} = 0.95\phi_m^{-1/2} d_{dis} \tag{9}$$

where ϕ_m is the volume fraction of the dispersed phase A.

Figure 11a shows the spin-diffusion plot for ER/EO30. The initial linear portion of the curve is extrapolated to give a value of 10.4 ms$^{1/2}$ for $(t_m^{s,0})^{1/2}$. Figure 11b shows a similar plot for the ER/EO80 blend, where a value of 2.8 ms$^{1/2}$ was obtained for $(t_m^{s,0})^{1/2}$. Table 2 lists all the parameters required for the spin-diffusion calculations; the calculated domain sizes and the long periods for ER/EO30 and ER/EO80 blends using values given in Table 2 are listed in Table 3.

Table 2. Volume Fraction, Line Widths, Spin−Lattice Relaxation Time, Spin-Diffusion Coefficients, and Equilibrium Mixing Time Used To Calculate the Domain Size

parameters[a]	ER/EO30	ER/EO80
ϕ_m	34.0	34.2
$\Delta\nu_{1/2}^{A}$ (kHz)	1.0	1.9
α (kHz)	59	62
$\Delta\nu_{1/2}^{B}$ (kHz)	41	41
D_A (nm^2/ms)	0.08	0.11
D_B (nm^2/ms)	0.32	0.32
T_1 (s)	0.76	0.90
$(t_m^{s,0})^{1/2}$ (ms$^{1/2}$)	10.4	2.8

[a] ϕ_m is the volume fraction of the dispersed phase A, i.e., EO30 or EO80 in the blends, which can be calculated from the 60:40 weight ratio of ER and block copolymer, as well as the density for ER, MDA, EO30, and EO80 of 1.17, 1.15,1.02, and 1.05 g/cm^3, respectively. $\Delta\nu_{1/2}^{A}$ and α for mobile A phase (i.e., EO30 or EO80), and $\Delta\nu_{1/2}^{B}$ for rigid B (i.e., ER) phase were determined by 2D WISE spectra as shown in Figure 7. D_A and D_B denote the spin-diffusion coefficients of the dispersed phase, EO30 or EO80, in the blends and the rigid ER phase, respectively. The spin−lattice relaxation time, T_1, were measured by means of the inversion recovery method.

Table 3. Domain Size (d_{dis}), Long Periods (d_{long}), and Interphase Thickness (d_{itp}) for ER/EO30 and ER/EO80 Blends Measured by Proton Spin-Diffusion Experiments

sample	ER/EO30	ER/EO80
ϵ	2	2
d_{dis} (nm)	8.9	2.7
d_{long} (nm)	14.4	4.3
d_{itp} (nm)	0.6	0.4

In Table 2, the calculated spin-diffusion coefficients for the mobile phase (0.08, 0.11 nm^2/ms) and the rigid phase (0.32, 0.32 nm^2/ms) for ER/EO30 and ER/EO80, respectively, are in good agreement with previous determined values.[35] In Table 3, the dimensionality of the system was chosen as $\epsilon = 2$, which is based on previously reported TEM results for the same samples. It was shown that wormlike micelles were formed for ER/EO30 and ER/EO80 blends containing 40 wt % triblock copolymers.[7] The calculated domain size from spin diffusion for ER/EO30 is 8.9 nm, and the long period is 14.4 nm. This result is in good agreement with SAXS result of 14.7 nm, shown in Figure 4, and also in good agreement with the value reported by Guo et al. on the same samples using SAXS (15.1 nm) and TEM experiments.[7] The calculated domain sizes and the long period for ER/EO80 blend are 2.7 and 4.3 nm, respectively, which are smaller than the corresponding values for the ER/EO30 blend. These spin-diffusion experiments provide convincing evidences for the existence of microphase separation on the nanoscale of 4−15 nm in the two blends. It is interesting to notice that the domain size in ER/EO80 is much smaller than that in ER/EO30, which could be attributed to the good miscibility of the PEO block with ER matrix and higher PEO content in EO80. SAXS is generally used for systems with a good electron density contrast between components. In previous work on ER/EO80, SAXS was unable to determine the length scale in this blend due to the

low contrast of the sample,[7] whereas the spin-diffusion NMR experiment can still quantitatively determine the domain size on a scale of several nanometers. In the above section of ^{1}H experiments, we have observed the large line broadening of the mobile phase in ER/EO80 as compared with ER/EO30. Because of the smaller domain size of ER/EO80 (2.7 nm), there would be much increased internal surfaces, to which more of the mobile chains can be attached to; thus, the corresponding line width would be greatly broadened than that of ER/EO30 (8.9 nm).

Since the domain size of the dispersed phase, d_{dis}, in ER/EO30 and ER/EO80 were determined, the interphase thickness, d_{itp}, for these blends can then be directly determined from eq 4. For ER/EO30, $d_{itp} = 0.07d_{dis} \approx 0.6$ nm, and for ER/EO80, $d_{itp} = 0.13d_{dis} \approx 0.4$ nm. It is interesting to notice that, despite the domain size of ER/EO30 being 3 times larger than that of ER/EO80, the interphase thickness of the two blends is only slightly different. The results based on the NMR analysis clearly indicate that, although the PEO volume fraction of the block copolymer can significantly affect the domain size of the blend, it has only small effect on the interphase thickness in the blend. To the best of our knowledge, the quantitative results about the interphase in PEO-containing block copolymer/ER blends have not been reported prior to this study.

Comparison with Related Work on Thermoset Blends with ER and PEO-Containing Block Copolymers. It is interesting to compare the present results with recent studies of PEO-containing block copolymer/ER thermoset blends. In the DSC study of the same ER/EO30 and ER/EO80 blends, Guo et al.[7] concluded that ER/EO30 and ER/EO80 blends containing 40 wt % copolymers were microphase separated; the PPO blocks form a separated microphase whereas ER and the PEO blocks, which are miscible, form another microphase. The PEO block of the copolymer was thought to be completely dissolved in the cured ER-rich microphase with EO30 or EO80 content lower than 50 wt %. This conclusion is not consistent with our present NMR results. Instead, the NMR studies demonstrate that part of the PEO blocks are repelled from the rigid ER matrix upon curing, as indicated by the large PEO mobility. Therefore, we can conclude that the PEO blocks are partially miscible with the cured-ER phase in these blends.

The discrepancy of these two studies could be due to the interpretation of the DSC experiments. The reported conclusion that the PEO blocks were completely dissolved in the cured EP was based on the following two evidences.[7] The first one is that no melting peak of PEO blocks was observed in the DSC experiments at the second scan of the sample and the first scan for as-prepared sample. The second one is that the corresponding samples were transparent. One could argue that the disappearance of the PEO melt point does not provide a strong evidence to support the conclusion that PEO is miscible with ER. Because PEO can be completely amorphous and mobile enough to exhibit a glass transition close to that of PPO,[28] the mobile PEO cannot be well distinguished with the mobile PPO in a DSC measurement. For example, we indeed observed one weak glass transition at −64 and −38 °C for ER/EO30 and ER/EO80, respectively, as shown in Figure 3. For the second evidence, one can argue that the blend would be transparent if the blend undergoes microphase separation on a nanoscale.

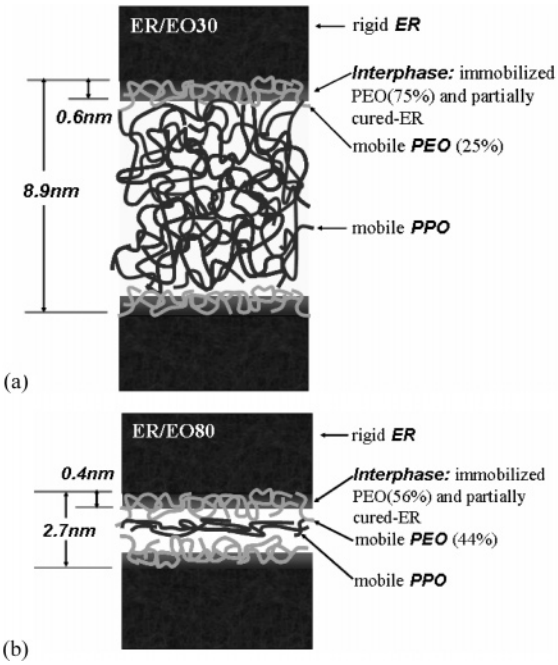

Figure 12. Schematic illustration of the suggested model for the heterogeneous dynamics, miscibility, and microdomain structure in (a) ER/EO30 and (b) ER/EO80 blends.

The present results are further supported by the work on MDA-cured ER/PEO−PPO blends reported by Mijovic et al. using DSC and dielectric relaxation spectroscopy (DRS) techniques.[6] They concluded that PEO gradually separated from the cured-ER matrix during some "critical" stage of cure in this nanostructured blend. They also suggested that a "middle layer" was likely to contain PEO mixed with some partially cured-ER network. In the studies of ER/PEO−PEP blends by Bates et al.,[4] it was found that the PEO phase was selectively swollen with the low molecular weight epoxy resins before curing. They suggested that PEO was locally expelled from the epoxy matrix upon curing, and this could be observed directly using TEM. They also found other evidence for the existence of a pure PEO interphase, i.e., their DSC measurements of a weak melt peak for PEO showing that a crystalline PEO region was present in the cured composite. The expulsion of the PEO could be attributed in part to the increased molecular weight of the cured epoxy polymer. A "wet-brush" to "dry-brush" transition model of the phase separation and interphase structure of the block copolymer/ER blends were also proposed by Bates et al., which is consistent with the results from our NMR work for ER/PEO−PPO−PEO blends. The present NMR work further indicates that information about the interphase formed by amorphous PEO and immobilized ER can also be obtained by NMR for ER/PEO−PPO−PEO blends, even though no crystalline PEO region exists in the blends.

Suggested Model of the Dynamics and Microphase Structure. On the basis of the NMR and DSC experiments reported above, a possible model for the dynamics and microphase structure in the cured ER/PEO−PPO−PEO blends could be postulated (Figure 12). Before curing, the block copolymers are self-assembled in the ER matrix. The PEO blocks are swollen by the low molecular weight epoxy resin, or they

form wet brushes. Upon curing, the cross-linked rigid ER formed a separated microphase, while partial mobile PEO was locally expelled from the cured-epoxy matrix and formed another microphase with mobile PPO phase. A portion of immobilized PEO blocks were intimately mixed with the partially cured ER phase and formed an interphase region. With an increased volume fraction of PEO in the block copolymer, the domain size decreases, whereas the interphase thickness is only slightly changed. On the basis of this model, both the phase behavior and heterogeneous dynamics in these blends can be understood, and more importantly, the detailed quantitative information on the interphase for PEO-containing block copolymer/ER thermoset blends could be obtained.

Conclusions

Using a variety of solid-state NMR techniques, we have shown that detailed information about the heterogeneous dynamics, miscibility, microdomain, and interphase structures in ER/PEO−PPO−PEO blends can be obtained. A distinct dynamic difference between the cured-ER matrix and block copolymers was observed by 1D and 2D NMR experiments, indicating that these blends underwent phase separations and the formation of crystalline domains in PEO block was inhibited. ^{1}H spin-diffusion experiments with different filter strengths demonstrated that, for the ER/EO30 and ER/EO80 blends, about 75% and 56% immobilized PEO were intimately mixed with the partially cured-ER in the interphase region. The determined domain sizes were 8.9 and 2.7 nm for ER/EO30 and ER/EO80, respectively, whereas the corresponding interphase thicknesses were 0.6 and 0.4 nm, which were only slightly different. These NMR results unambiguously demonstrate that PEO blocks were not completely dissolved in the cured-ER matrix. Rather, the EO blocks are partial miscible with the cured-ER matrix. Upon curing, the cross-linked rigid ER formed a separated microphase, while the part of the mobile PEO was locally expelled from the cured-ER matrix and formed another microphase with the mobile PPO. The residual immobilized PEO blocks were intimately mixed with the partially cured-ER phase, and they formed an interphase region. It is also concluded that with increasing the volume fraction of PEO in the block copolymer the domain size obviously decreased, whereas the interphase thickness is only slightly changed.

Acknowledgment. This work was supported by National Natural Science Foundation of China (Grants 20374031, 20373029, 20474034, 20233030, and 20274020), the Joint-Research Foundation of the Nankai and Tianjin Universities by the Chinese Ministry of Education, and the Foundation for University Key Teacher by the Chinese Ministry of Education (GG-703-10055-1008).

References and Notes

(1) (a) Stupp, S. I.; LeBonheur, V.; Walker, K.; Li, L. S.; Huggins, K.; Keser, M.; Amstutz, A. *Science* **1997**, *276*, 384. (b) Park, M.; Harrison, C.; Chaikin, P. M.; Register, R. A.; Adamson, D. H. *Science* **1997**, *276*, 1401. (c) Goldacker, T.; Abetz, V.; Stadler, R.; Erukhimovich, I.; Leibler, L. *Nature (London)* **1999**, *398*, 137.

(2) (a) Bates, F. S.; Fredrickson, G. H. *Annu. Rev. Phys. Chem.* **1990**, *41*, 525. (b) Fredrickson, G. H.; Bates, F. S. *Annu. Rev. Mater. Sci.* **1996**, *26*, 501. (c) Hadjichristidis, N.; Pispas, S.; Floudas, G. *Block Copolymers: Synthetic Strategies, Physical Properties, and Applications*; John Wiley & Sons: New York, 2002.

(3) (a) Hamley, I. W. *The Physics of Block Copolymers;* Oxford University Press: Oxford, 1998. (b) Winey, K. I.; Thomas, E. L.; Fetters, L. J. *Macromolecules* **1992**, *25*, 2645.

(4) (a) Lipic, P. M.; Bates, F. S.; Hillmyer, M. A. *J. Am. Chem. Soc.* **1998**, *120*, 8963. (b) Hillmyer, M. A.; Lipic, P. M.; Hajduk, D. A.; Almdal, K.; Bates, F. S. *J. Am. Chem. Soc.* **1997**, *119*, 2749.

(5) (a) Grubbs, R. B.; Dean, J. M.; Broz, M. E.; Bates, F. S. *Macromolecules* **2000**, *33*, 9522. (b) Grubbs, R. B.; Dean, J. M.; Bates, F. S. *Macromolecules* **2001**, *34*, 8593. (c) Dean, J. M.; Verghese, N. E.; Pham, H. Q.; Bates, F. S. *Macromolecules* **2003**, *36*, 9265.

(6) Mijovic, J.; Shen, M.; Sy, J. W.; Mondragon, I. *Macromolecules* **2000**, *33*, 5235.

(7) Guo, Q.; Thomann, R.; Gronski, W. *Macromolecules* **2002**, *35*, 3133.

(8) (a) Hussein, I. A. *Macromolecules* **2003**, *36*, 4667. (b) Yi, J.; Goh, S. H.; Wee, A. T. S. *Macromolecules* **2001**, *34*, 4662, 7411. (c) Kuo, S. W.; Chang, F. C. *Macromolecules* **2001**, *34*, 5224. (d) Eisenbach, C. D.; Hoffman, J.; Goldel, A.; Noolandi, J.; Shi, A.-C. *Macromolecules* **1999**, *32*, 1463.

(9) (a) Guo, Q.; Thomann, R.; Gronski, W. *Macromolecules* **2003**, *36*, 3635. (b) Guo, Q.; Harrats, C.; Groeninckx, G.; Koch, M. J. H. *Polymer* **2001**, *42*, 4127.

(10) (a) Zhu. L.; Huang, P.; Chen, W. Y.; Ge, Q.; Quirk, R. P.; Cheng, S. Z. D.; Thomas, E. L.; Lotz, B.; Hsiao, B. S.; Yeh, F.; Liu, L. *Macromolecules* **2002**, *35*, 3553. (b) Court, F.; Hashimoto, T. *Macromolecules* **2002**, *35*, 2566.

(11) (a) Hu, W. G.; Schmidt-Rohr, K. *Polymer* **2000**, *41*, 2979. (b) VanderHart, D. L.; Alamo, R. G.; Nyden, M. R.; Kim, M.-H.; Mandelkern, L. *Macromolecules* **2000**, *33*, *6078*.

(12) (a) Werkhoven, T. M.; Mulder, F. M.; Zune, C.; Terome, R.; de Groot, H. J. M. *Macromol. Chem. Phys.* **2003**, *204*, 46. (b) Kim, C.; Lee, S. C.; Kwon, I. C. *Macromolecules* **2002**, *35*, 193. (c) Kryz, J.; Masar, B.; Plestil, J. *Macromolecules* **1998**, *31*, 41.

(13) (a) VanderHart, D. L.; Feng, Y.; Han, C. C.; Weiss, R. A. *Macromolecules* **2000**, *33*, 2206. (b) VanderHart, D. L.; Manley, R. S. J.; Barnes, J. D. *Macromolecules* **1994**, *27*, 2826. (c) Mulder, F. M.; Jansen, B. J. P.; Lemstra, P. J.; Meijer, H. E. H.; de Groot, H. J. M. *Macromolecules* **2000**, *33*, 457. (d) Cho, G.; Natansohn, A. *Chem. Mater.* **1997**, *19*, 148. (f) Wagler, T.; Rinaldi, L.; Han, C. D.; Chun, H. *Macromolecules* **2000**, *33*, 1778.

(14) McCormick, M.; Smith, R. N.; Graf, R.; Barrett, C. J.; Reven, L.; Spiess, H. W. *Macromolecules* **2003**, *36*, 3616.

(15) (a) Paul, S. M. D.; Zwanziger, J. W.; Ulrich, R.; Wiesner, U.; Spiess, H. W. *J. Am. Chem. Soc.* **1999**, *121*, 5727. (b) VanderHart, D. L.; Asano, A.; Gilman J. W. *Chem. Mater.* **2001**, *13*, 3781, 3796. (c) Hou, S. S.; Beyer, F. L.; Schmidt-Rohr, K. *Solid State Nucl. Magn. Reson.* **2002**, *22*, 110.

(16) Tonelli, A. E. *NMR Spectroscopy and Polymer Microstructure*; VCH: New York, 1989.

(17) Clauss, J.; Schmidt-Rohr, K.; Spiess, H. W. *Acta Polym.* **1993**, *44*, 1.

(18) Landfester, K.; Spiess, H. W. *Acta Polym.* 1**998**, *49*, 451.

(19) (a) VanderHart, D. L. *Macromolecules* **1994**, *27*, 2837. (b) Cherry, B. R.; Fujimoto, C. H.; Cornelius, C. J.; Alam, T. M. *Macromolecules* **2005**, *38*, 1201.

(20) Mirau, P. A.; Yang, S. *Chem. Mater.* **2002**, *14*, 249.

(21) Schmidt-Rohr, K.; Spiess, H. W. *Multidimensional Solid-State NMR and Polymers*; Academic Press: San Diego, 1994.

(22) (a) Schmidt-Rohr, K.; Clauss, J.; Spiess, H. W. *Macromolecules* **1992**, *25*, 3273. (b) Tekely, P.; Palmas, P.; Mutzenhart, P. *Macromolecules* **1993**, *26*, 7363.

(23) Mellinger, F.; Wilhelm, M.; Spiess, H. W. *Macromolecules* **1999**, *32*, 4686.

(24) (a) Cai, W. Z.; Schmidt-Rohr, K.; Egger, N.; Gerharz, B.; Spiess, H. W. *Polymer* **1993**, *34*, 267. (b) Egger, N.; Schmidt-Rohr, Blumich, B.; Domke, W. D.; Stapp, B. *J. Appl. Polym. Sci.* **1992**, *44*, 289.

(25) Neagu, C.; Puskas, J. E.; Singh, M. A.; Natansohn, A. *Macromolecules* **2000**, *33*, 5976.

(26) Bovey, F. A.; Mirau, P. A. *NMR of Polymers;* Academic Press: New York, 1996.

(27) (a) Brown, S. P.; Schnell, I.; Spiess, H. W. *J. Am. Chem. Soc.* **1999**, *121*, 6712. (b) English, A. D.; Debowski, C. *Macromolecules* **1984**, *17*, 446. (c) Graf, R.; Heuer, A.; Spiess, H. W. *Phys. Rev. Lett.* **1998**, *80*, 5738.

(28) Brandrup, J.; Immergut, E. H. *Polymer Handbook*, 3rd ed.; Brandrup, J., Immergut, E. H., Eds.; John Wiley & Sons: New York, 1989.
(29) (a) Liu, R. Y. F.; Bernal-Lara, T. E.; Hiltner, A.; Baer, E. *Macromolecules* **2004**, *37*, 6972. (b) Spontak, R. J.; Zielinski, J. M. *Macromolecules* **1993**, *26*, 396. (c) Yeung, C.; Shi, A.-C. *Macromolecules* **1999**, *32*, 3637.
(30) (a) Ivanov, D. A.; Pop, T.; Yoon, D. Y.; Jonas, A. M. *Macromolecules* **2002**, *35*, 9813. (b) Lestriez, B.; Chapel, J.; Gerard, J. *Macromolecules* **2001**, *34*, 1204.
(31) (a) Landfester, K.; Boeffel, C.; Lambla, M.; Spiess, H. W. *Macromolecules* **1996**, *29*, 5972. (b) Mellinger, F.; Wilhelm, M.; Spiess, H. W.; Baumstark, R.; Haunschild, A. *Macromol. Chem. Phys.* **1999**, *200*, 719. (c) Jack, K. S.; Wang, J.; Natansohn, A.; Register, R. A. *Macromolecules* **1998**, *31*, 3282. (d) Wang, J.; Jack, K. S.; Natansohn, A. *J. Chem. Phys.* **1997**, *107*, 1016.
(32) Domjan, A.; Erdodi, G.; Wilhelm, M.; Neidhofer, M.; Landfester, K.; Ivan, B.; Spiess, H. W. *Macromolecules* **2003**, *36*, 9107.
(33) VanderHart, D. L.; McFadden, G. B. *Solid State Nucl. Magn. Reson.* **1996**, *7*, 45.
(34) Demco, D. E.; Johanson, A.; Tegenfeldt, J. *Solid State Nucl. Magn. Reson.* **1995**, *4*, 13.
(35) (a) Brus, J.; Dybal, J.; Schmidt, P.; Kratochvil, J.; Baldrian, J. *Macromolecules* **2000**, *33*, 6448. (b) Clayden, N. J.; Nijs, C. L.; Eeckhaut, G. J. *Polymer* **1997**, *38*, 1011. (c) Clauss, J.; Schmidt-Rohr, K.; Adam, A.; Boeffel, C.; Spiess, H. W. *Macromolecules* **1992**, *25*, 5208. (d) Wilhelm, M.; Lehmann, S.; Jager, C.; Spiess, H. W. *Magn. Reson. Chem.* **1994**, *32*, S3.

MA0505979